Clay Minerals (2024), **59**, 26–38
doi:10.1180/clm.2024.4

CAMBRIDGE UNIVERSITY PRESS

Article

Adsorption of atrazine and paraquat on montmorillonite loaded with layered double hydroxide and active site energy distribution analysis

Rui Liu[1,2], Chao Ma[1], Huanliang Chen[1], Changsuo Li[1], Lei Zuo[2], Peng Zhang[2], Yaqing Wang[2] and Ru Wang[2]

[1]801 Institute of Hydrogeology and Engineering Geology, Shandong Provincial Bureau of Geology & Mineral Resources (Shandong Provincial Geo-Mineral Engineering Exploration Institute), Jinan, China and [2]School of Resources and Environmental Engineering, Shandong University of Technology, Zibo, China

Abstract

Clay minerals are effective adsorbents for the remediation of pesticides in wastewater due to their large superficial areas and excellent cation-exchange capabilities. However, this adsorption effect can be reduced by the accumulation of adsorbents on clay minerals, amongst other problems. Therefore, in this study, montmorillonite (Mnt) modified by layered double hydroxide (LDH) with different loading amounts was successfully prepared using an *in situ* method. The results from X-ray diffraction, Fourier-transform infrared spectrometry, Brunauer–Emmet–Teller (BET) and scanning electron microscopy analyses revealed that LDH structures were successfully combined with the Mnt layer and formed a porous structure. However, excess LDH still caused the aggregation and accumulation of layers. The adsorption performance of LDH@Mnt for atrazine (ATZ) and paraquat (PQ) was investigated, and the removal efficiency of the LDH@Mnt composite was higher than those of Mnt and LDH alone. The kinetic study revealed that the adsorption process fitted the pseudo-second-order model and internal diffusion model, and 3-LDH@Mnt had the greatest absorbability efficiency for both ATZ and PQ, indicating the adsorption process was controlled by the number of active sites of the adsorbent. The generalized Langmuir model accurately characterized the adsorption process of ATZ and PQ elimination in the adsorption isotherm investigation, indicating that the adsorption energies of the active sites on the adsorbents were different. 3-LDH@Mnt had better absorbability performance for ATZ/PQ, and the sorption capacities were 7.03 and 91.9 mg g^{-1}, respectively. According to site energy distribution theory, the amount of sorption sites of the composite adsorbent was large and the average adsorption energy was high, both of which being beneficial for the adsorption of ATZ and PQ. The effects of pH, coexisting anions and reuse experiments were also tested, indicating that the LDH@Mnt composite possessed high adsorption stability. This excellent removal performance represents a promising strategy for the remediation and elimination of pesticide contaminations from the environment.

Keywords: Adsorption; layered double hydroxide; montmorillonite; pesticides

(Received 30 October 2023; revised 1 February 2024; accepted 6 February 2024; Accepted Manuscript online: 19 February 2024; Associate Editor: Chunhui Zhou)

Agriculture is vital to social stability and economic development. In recent years, with the development of agriculture, the use of pesticides has shown an increasing trend year after year (Ionel *et al.*, 2019; Centner, 2021; Vasseghian *et al.*, 2022; Siddique *et al.*, 2023). The annual use of pesticides is close to 350 tons, but only ∼1% of pesticides reduce the effects of diseases and pests on crops, and most pesticides do not perform their intended role (Glaberman *et al.*, 2017; Valbuena *et al.*, 2021). The continuous exposure to residual pesticides in nature causes serious problems for non-target organisms (Mandal *et al.*, 2017). Moreover, the biochemical degradation performance of pesticides is poor, and pesticide residues in nature have negative impacts on soil and water environments (Chen *et al.*, 2019). In addition, pesticides pollute groundwater and soil, thus impacting humans, animals and ecosystems. Hence, it is of great importance to reduce concentrations of pesticides in the environment (Durán *et al.*, 2019). Many studies have used adsorption methods to remove pesticides with, for example, biochar, bentonite, zeolite and diatomaceous earth (Tsai *et al.*, 2005; Salvestrini *et al.*, 2010; Hernandes *et al.*, 2022).

Layered double hydroxide (LDH) is a form of adsorbent material with a special layered structure and physicochemical properties (Chen *et al.*, 2016; Liu *et al.*, 2022; Zheng *et al.*, 2022; Tian *et al.*, 2023). In this context, LDH, generally expressed as $[M^{2+}_{1-x}M_x{}^{3+}(OH)_2A_{x/n}{}^{n-}\cdot mH_2O]$, belongs to the category of anionic clays. Here, M^{2+} represents a metal ion, M^{3+} denotes the trivalent metal cation and A^{n-} signifies the interlayer anion on the equilibrium layer(Tao *et al.*, 2017, 2018; Huang *et al.*, 2022). LDH has garnered significant attention as a means of removing contaminants from the environment due to its simple preparation, flexible structure, chemical durability and large surface area (Wu *et al.*, 2023). However, LDH still has the disadvantages of strong aggregation and low porosity, which severely restrict the capacity of LDH to adsorb and remove pollutants (Dabizha & Kersten, 2022).

Corresponding author: Changsuo Li; Email: lics120@163.com
Cite this article: Liu R, Ma C, Chen H, Li C, Zuo L, Zhang P, Wang Y, Wang R (2024). Adsorption of atrazine and paraquat on montmorillonite loaded with layered double hydroxide and active site energy distribution analysis. *Clay Minerals* **59**, 26–38. https://doi.org/10.1180/clm.2024.4

Clay minerals exhibit a considerable specific surface area and ion exchange capacity, but the structure of clay minerals leads to their easy accumulation, and other problems also affect their adsorption capacity (Uygun *et al.*, 2023). Montmorillonite (Mnt) represents a typical 2:1 layered clay mineral, consisting of two silica tetrahedral sheets surrounding one octahedral sheet incorporating aluminium or magnesium (Semenkova *et al.*, 2018; Alexe-Ionescu *et al.*, 2019). The negative charges on the Mnt layer are created by isomorphic substitution mostly in the octahedral layer (Al Kausor *et al.*, 2022). Today, Mnt has been widely used as an adsorbent due to its large specific surface area, strong reuse ability, low cost and non-toxicity (la Cecilia & Maggi, 2016; Buchanan & Hiltbold, 2017; Silva *et al.*, 2020). Inorganic pillaring and organic modification are the main modification methods used to improve the properties or functions of Mnt. For inorganic modification to improve the adsorption ability of Mnt for contaminants, cations (such as Al^{3+} and Ti^{4+}) are introduced into the interlayers of Mnt, which possess high surface areas and large pore volumes. Organic surfactants are common modifiers applied in organic modification, which enhance the affinity of Mnt for organic contaminants (Ajala *et al.*, 2018; Boutaleb *et al.*, 2021; Al Kausor *et al.*, 2022). However, the utilization of Mnt as an adsorbent still has several disadvantages of easy layer stacking and poor porosity, significantly limiting its practical applicability in water treatment (Liao *et al.*, 2022; Mennas *et al.*, 2023). Based on the excellent physicochemical properties of LDH and Mnt, the problems of particle aggregation and layer stacking could be overcome *via* mutual benefits of LDH and Mnt layers.

Hence, in this study, the *in situ* growth of LDH on Mnt layers was achieved using the co-precipitation method, and the structure was examined using X-ray diffraction (XRD), Fourier-transform infrared (FTIR) spectroscopy, scanning electron microscopy (SEM) and Brunauer–Emmet–Teller (BET) analyses. Here, due to their wide usage and serious environmental impacts, the pesticides paraquat (PQ) and atrazine (ATZ) were employed as targeted contaminants. The adsorption efficiencies and adsorption processes of PQ and ATZ were investigated *via* kinetic and isothermal studies. The test data regarding isothermal adsorption were further analysed using the theory of site energy distribution, confirming their strong correlation with the generalized Langmuir model. Furthermore, the impacts of pH, coexisting ions and reuse tests of adsorption efficiency were investigated.

Materials and methods

Materials and apparatus

In the experiments, $Mg(NO_3)_2{\cdot}6H_2O$, $Al(NO_3)_3{\cdot}9H_2O$ and NaOH were all analytical grade and obtained from Aladdin Chemicals Co. Ltd (Shanghai, China). Mnt was purchased from Yihe Pharmaceutical Co. Ltd. ATZ and PQ were obtained from Shandong Binnong Technology Co. Ltd. The half-life of ATZ is 60–150 days and the half-life of PQ is 84 h. The water solubilities for ATZ and PQ are 70 mg L^{-1} and 620 g L^{-1}, respectively.

Synthesis process of LDH@Mnt

0.4 g Mnt was mixed with 300 mL deionized water to obtain a suspension, and the suspension was placed in a high-speed mixer for 30 min. Mixed brine solution with $n(Mg^{2+})/n(Al^{3+})$ = 2:1 was dissolved in 100 mL deionized water and added to the Mnt suspension. Then, 0.5 M NaOH solution was added dropwise to the suspension whilst stirring until reaching pH 10. The obtained suspension was left for 24 h, centrifuged at 8000 rpm for 5 min, washed and then desiccated at 80°C. The Mg^{2+} molar amounts in mixed salt solution were 1, 2, 3, 4 and 5 mmol, and the produced specimens were recorded as 1-LDH@Mnt, 2-LDH@Mnt, 3-LDH@Mnt, 4-LDH@Mnt and 5-LDH@Mnt, respectively.

Adsorption experiments of ATZ and PQ

In the adsorption isotherm experiment, 100 mg of adsorbent was combined with 25 mL of ATZ or PQ. The initial concentrations of ATZ or PQ were 25–300 mg L^{-1} in the solution with a water:ethanol ratio of 9:1. The conical flask containing the absorbent was shaken at 25°C in a constant-temperature oscillator for 5 h. The mixed solution underwent centrifugation and the overflow solution was taken for examination. For the dynamic experiment, solutions of ATZ and PQ with initial concentrations of 100 mg L^{-1} were prepared. Subsequently, 1 g of adsorbent was introduced into a conical flask along with 250 mL of ATZ or PQ solution. ATZ and PQ solutions were taken out at predetermined time (10–300 min), and 5 mL of overflow solution was centrifuged for testing using high-performance liquid chromatography (HPLC). The concentration of ATZ and PQ was determined using a HPLC device equipped with a C18 reverse chromatographic column (250 mm × 4.6 mm inner diameter, 5 µm particle size), and the mobile phase was a mixture of methanol and 0.1% formic acid aqueous solution. The flow rate was 1 mL min^{-1} and the oven temperature was 40°C.

The effects of pH, coexisting ions and reuse experiments

In the pH experiment, 100 mg of the 3-LDH@Mnt sample was introduced into conical flasks containing 25 mL of ATZ/PQ solutions with concentrations of 100 mg L^{-1}. The initial pH of the ATZ and PQ solutions was regulated to 3, 5, 7 or 9 using 0.1 M HCl and NaOH solutions. The experimental procedure remained consistent with the adsorption experiment. Additionally, to assess the impacts of anions (Cl^-, NO_3^{2-}, SO_4^{2-} CO_3^{2-}) and cations (Na^+, K^+, Mg^{2+} and Ca^{2+}) on the adsorption of ATZ and PQ, solutions with concentrations of 100 mg L^{-1} for each ion were added to the original ATZ and PQ solutions. The reusability of 3-LDH@Mnt was also studied. Sample 3-LDH@Mnt (100 mg) was added to conical flasks containing 25 mL of ATZ/PQ solutions with concentrations of 100 mg L^{-1} and then desorbed in a 10 mL solution of NaOH with a concentration of 0.1 M. After desorption, the sample underwent a repeat of the above process (shown in Fig. S1). The adsorption experiments of 3-LDH@Mnt for ATZ and PQ were repeated five times and the results recorded each time.

Characterization methods

XRD traces of all samples before and after adsorption were obtained using powder XRD (Japan Rigaku D/MaxgA) with Cu-*K*α radiation. FTIR spectroscopy was used to characterize the principal functional groups of the materials using the KBr pellet method collected in the range of 4000 to 500 cm^{-1}. The BET specific surface area and pore-size distribution were obtained using N_2 adsorption/desorption analysis with a Micromeritics ASAP 2460. SEM images of the surface contours and of the micro-mechanism that the samples underwent were acquired

https://doi.org/10.1180/clm.2024.4 Published online by Cambridge University Press

using a Hitachi H-8010 SEM device. HPLC was performed using a 1260 Infinity II liquid chromatography system purchased from Agilent.

Results and discussion

Characterization of the LDH@Mnt

XRD traces of Mnt, LDH, 1-LDH@Mnt, 3-LDH@Mnt and 5-LDH@Mnt are shown in Fig. 1a. In the XRD trace of LDH, the characteristic peaks of (003), (006), (018) and (013) located at 11.4, 23.1, 34.4 and 61.5°2θ, representing the LDH crystal structure, were observed. In the XRD trace of Mnt, the characteristic peaks of (001), (002) and (010) are located at 7.8, 20.1 and 63.3°2θ. In the XRD traces of 1-LDH@Mnt, 3-LDH@Mnt and 5-LDH@Mnt, the characteristic peaks of Mnt and LDH were present in all of compound samples, demonstrating the successful combination of LDH and Mnt, and there was no phase transition during the preparation process (Wu *et al.*, 2023).

The samples of Mnt, LDH, 1-LDH@Mnt, 3-LDH@Mnt and 5-LDH@Mnt were tested using FTIR spectroscopy, and the results are shown in Fig. 1b. The peaks at 3624, 3444 and 1631 cm^{-1} were attributed to the hydroxyl stretching vibration (Wu *et al.*, 2023), the interlayer water stretching vibration and the bending vibration of Mnt and LDH, respectively. The high-intensity absorption band at 1029 cm^{-1} represent the characteristic Si–O peak in the silico-oxygen tetrahedron of Mnt (Wu *et al.*, 2023). The characteristic peaks at ~1369 and 800 cm^{-1} represent the N–O vibration of nitrate in the interlayer and the metal oxide vibration of LDH, respectively. In the results for 1-LDH@Mnt, 3-LDH@Mnt and 5-LDH@Mnt, the characteristic peaks of Mnt and LDH in all of the composite samples were observed, indicating that the LDH structure was loaded onto Mnt using *in situ* method and that the composite samples were prepared successfully.

The specific surface and pore radius distribution of Mnt, 1-LDH@Mnt, 3-LDH@Mnt and 5-LDH@Mnt were analysed using N_2 adsorption/desorption experiments, and the results are shown in Fig. S2 and Table 1. Compared with Mnt, the specific surfaces of the LDH@Mnt samples were greater because the mutual support of the LDH and Mnt layers improved the pore structure, and the specific area of 3-LDH@Mnt was higher than those of the other samples. In addition, from the pore-size distribution results, 3-LDH@Mnt also possessed a greater micropore structure than the other samples, indicating that the composite sample had a favourable pore structure and was conducive to the adsorption of pesticides.

Table 1. Structural characteristics of Mnt, 1-LDH@Mnt, 3-LDH@Mnt and 5-LDH@Mnt.

Sample	Surface area (mg^2 g^{-1})	Pore diameter (nm)
Mnt	17.59	12.84
LDH	19.32	11.09
1-LDH@Mnt	23.46	12.08
3-LDH@Mnt	62.57	6.82
5-LDH@Mnt	48.32	9.27

The morphologies of samples 1-LDH@Mnt, 3-LDH@Mnt, 5-LDH@Mnt and Mnt were investigated using SEM, and the findings are presented in Fig. 2. In Fig. 2a,b, both LDH and Mnt layers are presented, revealing that the composite sample of LDH@Mnt was synthesized successfully using the *in situ* method. Compared with the morphology of Mnt, the presence of LDH loosened the Mnt layers. However, on account of the low loading amount of LDH, the structure of LDH with its small size was formed on the surface of Mnt. The LDH and Mnt layers could not support each other, resulting in the layers collapsing and becoming stacked. As shown in Fig. 2c,d, with the increased LDH loading amount and the growth of the formed LDH structure, LDH and Mnt layers supported and interpenetrated each other to form a porous structure, overcoming the problems of particle aggregation and layer stacking. Hence, in the 3-LDH@Mnt sample, Mnt modified by the LDH layer demonstrated a significantly enlarged specific surface area, increased structural stability and greater numbers of exposed active sites. However, with further increases of LDH loading (Fig. 2e,f), the amount of LDH became excessive and accumulated on the surface of Mnt, and these could not support Mnt layers and gradually stacked together, revealing that excess LDH-modified Mnt still underwent aggregation and the accumulation of layers.

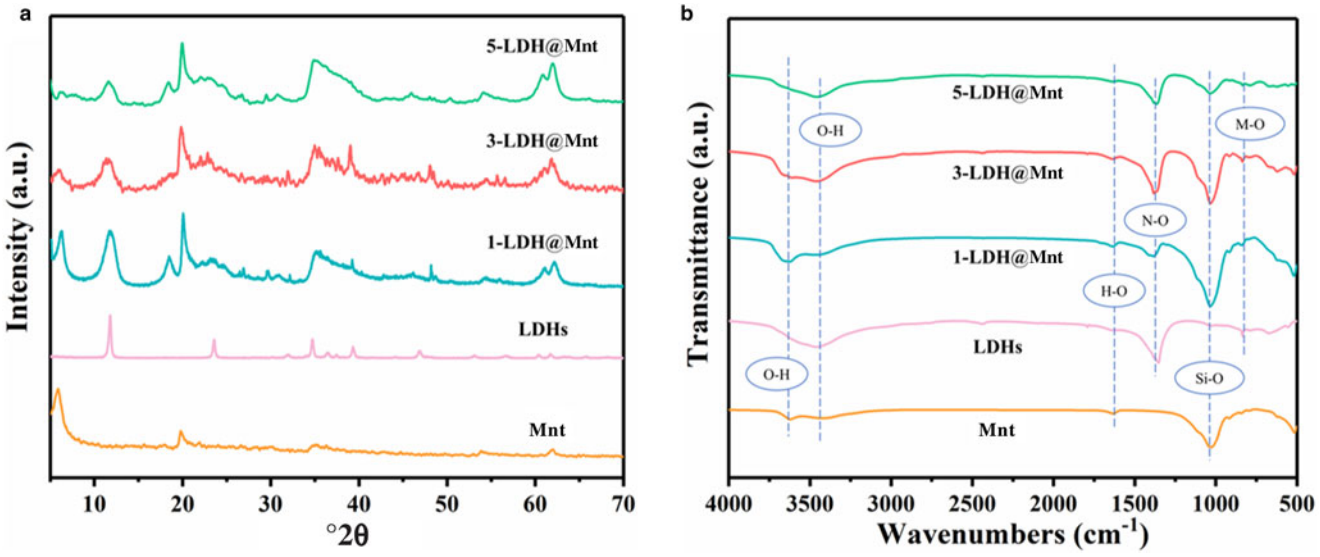

Figure 1. (a) XRD traces and (b) FTIR spectra of Mnt, LDH, 1-LDH@Mnt, 3-LDH@Mnt and 5-LDH@Mnt.

https://doi.org/10.1180/clm.2024.4 Published online by Cambridge University Press

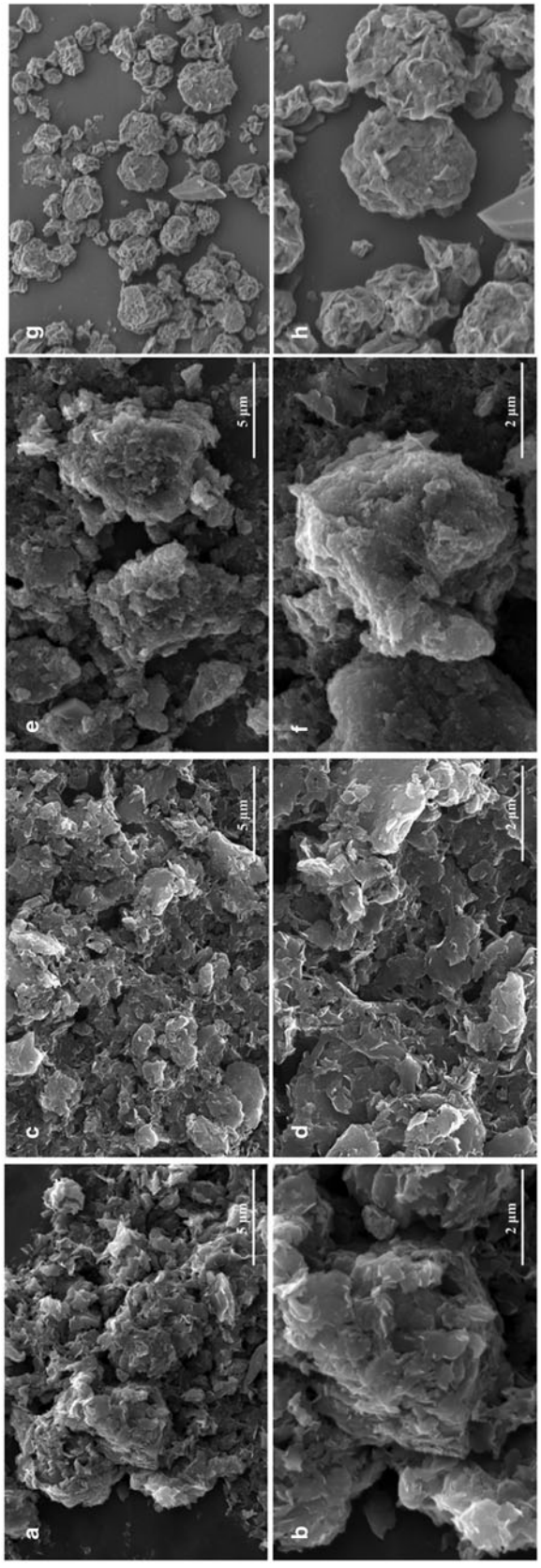

Figure 2. SEM images of (a,b) 1-LDH@Mnt, (c,d), 3-LDH@Mnt, (e,f) 5-LDH@Mnt and (g,h) Mnt.

Adsorption kinetics

The adsorption kinetics of ATZ and PQ by Mnt, LDH and composite samples over time were investigated, and the results are shown in Fig. 3. During the sorption process, the removal of ATZ and PQ was rapid in the first hour, and then the rate slowed down until adsorption equilibrium was established at 3 h. During the process of ATZ and PQ removal, the removal rate was one of the means used to evaluate adsorbent properties because it had a large effect on the removal efficiency and depended on the properties of the material. Therefore, we applied the quasi-first-order kinetic model (Equation 1), quasi-second-order kinetic model (Equation 2) and interdiffusion model (Equation 3) to analyse the experimental data. The average relative error (ARE) was utilized to assess the matching quality (Equation 4). A lesser ARE value indicates a better fitting degree.

$$Q_t = Q_e(1 - e^{-tk_1}) \tag{1}$$

$$Q_t = \frac{Q_e t}{(1/k_2 Q_e) + t} \tag{2}$$

$$Q_t = K_i t^{0.5} + C \tag{3}$$

$$\text{ARE} = \frac{100}{n}\sum_{i}^{n}\left|\frac{Q_{i,\text{model}} - Q_{i,\text{exp}}}{Q_{i,\text{exp}}}\right| \tag{4}$$

where Q_t and Q_e (mg g^{-1}) is the amount of adsorbed ATZ and PQ at time t and equilibrium, respectively. k_1 and k_2 (mL mg^{-1} h^{-1}) represent the constants of the pseudo-first-order model and the pseudo-second-order model, respectively. K_i (mg g^{-1} $h^{-1/2}$) represents the rate constant of internal diffusion and C is the coefficient of internal diffusion. $Q_{i,\ model}$ is each Q (mg g^{-1}) value forecasted by the predicting model, $Q_{i,exp}$ is each Q (mg g^{-1}) measured experimentally and n is the number of experimental points.

The fitted results of these models are displayed in Figs 3 & S3, and the calculated kinetic equation parameters are listed in Table 2. Based on the ARE and R^2 values of the models, all of the samples showed better-fitting results to the adsorption testing data of ATZ and PQ according to the pseudo-second-order kinetic model. Additionally, the equilibrium removal values of ATZ and PQ, calculated using the pseudo-second-order model, closely matched the experimental data. The superior fit provided by the pseudo-second-order kinetic model suggests that the adsorption of ATZ and PQ is primarily governed by the number of adsorption sites on the adsorbent. Compared to Mnt and LDH, the adsorption capacities of compound adsorbents for ATZ and PQ were much larger, and 3-LDH@Mnt possessed the greatest removal efficiency. These results indicated that in composite adsorbents the mutually supported LDH and Mnt layers formed a porous structure and provided more accessible adsorption sites for ATZ and PQ removal. When the loading amount of LDH was small, the adsorption sites for ATZ and PQ were insufficient. However, overloading LDH on the Mnt surface resulted in excessive aggregation, which reduced the exposure of biosorption sites and lowered the adsorption amount. These variations in removal capabilities corresponded to changes in the shape of

https://doi.org/10.1180/clm.2024.4 Published online by Cambridge University Press

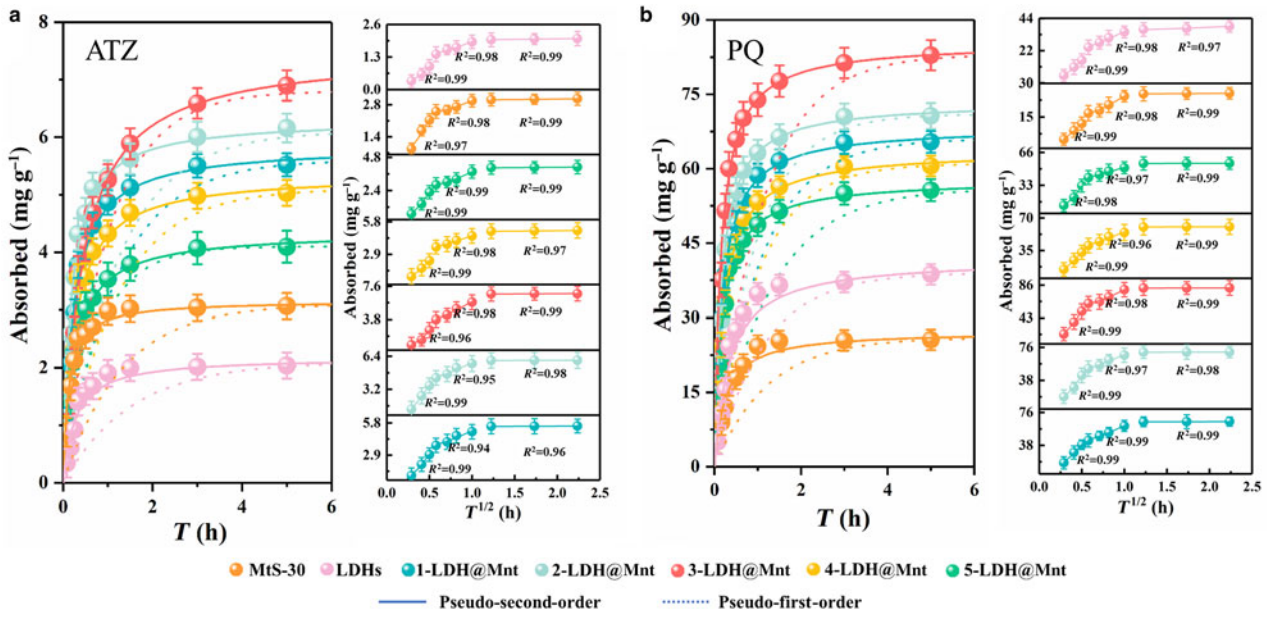

Figure 3. Kinetics of (a) ATZ and (b) PQ on Mnt, LDH, 1-LDH@Mnt, 2-LDH@Mnt, 3-LDH@Mnt, 4-LDH@Mnt and 5-LDH@Mnt fitted with pseudo-first-order, pseudo-second-order and internal diffusion models.

the composite adsorbents as well as increases in their specific surface area.

The internal diffusion model was also used to analyse the test data, and the results of ATZ and PQ removal are shown in Fig. 3 and Table 3. From internal diffusion model results, at the beginning ATZ/PQ was first adsorbed on the surface of the adsorbent. Then, over time, ATZ/PQ molecules gradually diffused inside the adsorbent. Finally, adsorption equilibrium was reached. As a result, the adsorption process can be separated into three stages: surface diffusion, interdiffusion and adsorption equilibrium, demonstrating that interior biosorption sites are exposed and gradually become occupied during the sorption process. In composite sample, LDH and Mnt layers mutually supported each other to generate a pore structure, which led to more ATZ and PQ molecules diffusing into the interior of these samples and increased the diffusion rate of ATZ and PQ molecules during the adsorption process. The value of K_{d2} represents the adsorption rate of internal diffusion, and sample 3-LDH@Mnt possessed the highest value of K_{d2}, revealing that this composite adsorbent has the most beneficial internal structure that is conducive to the removal of ATZ/PQ. Furthermore, from the linear fitting of intraparticle diffusion results we can see that not all samples' fitted curves pass through the origin, indicating that the adsorption of ATZ and PQ molecules was controlled by multiple steps.

Adsorption isotherms

The influence of the initial concentration on the removal of ATZ and PQ by Mnt, LDH and composite adsorbents was investigated. With increasing initial concentration, the adsorption amounts of ATZ and PQ for all samples increased initially, and then the adsorption amounts gradually reached equilibrium. To further analyse the mechanism of the removal process, Langmuir

Table 2. Pseudo-first-order model and pseudo-second-order model kinetic parameters of ATZ and PQ adsorbed by Mnt, LDH, 1-LDH@Mnt, 2-LDH@Mnt, 3-LDH@Mnt, 4-LDH@Mnt and 5-LDH@Mnt.

Contaminant	Absorbent	Pseudo-first-order model				Pseudo-second-order model			
		K_1 (h^{-1})	Q_e (mg g^{-1})	R^2	ARE	K_2 (g mg^{-1} h^{-1})	Q_e (mg g^{-1})	R^2	ARE
ATZ	Mnt	0.013	6.83	0.73	49.9	0.045	2.98	0.99	17.2
	LDH	0.011	6.12	0.72	47.7	0.028	2.02	0.99	15.5
	1-LDH@Mnt	0.014	5.52	0.74	61.8	0.013	5.51	0.99	42.8
	2-LDH@Mnt	0.013	4.93	0.69	59.6	0.014	5.92	0.99	49.8
	3-LDH@Mnt	0.017	4.04	0.77	25.2	0.005	6.8	0.99	10.3
	4-LDH@Mnt	0.014	2.98	0.78	41.7	0.012	4.96	0.99	13.1
	5-LDH@Mnt	0.021	2.01	0.89	28.6	0.016	3.98	0.99	11.4
PQ	Mnt	0.014	26.2	0.73	28.4	0.002	27.3	0.99	15.5
	LDH	0.014	39.5	0.89	29.1	0.001	41.8	0.99	16.8
	1-LDH@Mnt	0.015	66.3	0.75	23.9	0.001	68.5	0.99	17.3
	2-LDH@Mnt	0.017	71.1	0.74	31.2	0.001	73.5	0.99	23.4
	3-LDH@Mnt	0.015	83.2	0.69	17.3	0.001	85.5	0.99	10.9
	4-LDH@Mnt	0.017	61.2	0.78	33.9	0.001	63.7	0.99	21.3
	5-LDH@Mnt	0.013	56.1	0.70	29.3	0.002	57.8	0.99	18.6

https://doi.org/10.1180/clm.2024.4 Published online by Cambridge University Press

Table 3. Parameters of the internal diffusion model of ATZ and PQ adsorbed by Mnt, LDH, 1-LDH@Mnt, 2-LDH@Mnt, 3-LDH@Mnt, 4-LDH@Mnt and 5-LDH@Mnt.

		Internal diffusion model								
		Surface diffusion			Internal diffusion			Adsorption equilibrium		
Contaminant	Absorbent	K_{d1} (mg g^{-1} $h^{-1/2}$)	C_1	R^2	K_{d2} (mg g^{-1} $h^{-1/2}$)	C_2	R^2	K_{d3} (mg g^{-1} $h^{-1/2}$)	C_3	R^2
ATZ	Mnt	0.73	0.81	0.97	0.122	22.4	0.98	0.0022	30.1	0.99
	LDH	0.67	0.42	0.99	0.124	12.0	0.98	0.0021	19.8	0.99
	1-LDH@Mnt	1.91	1.32	0.99	0.316	32.1	0.94	0.0018	54.8	0.96
	2-LDH@Mnt	2.23	1.83	0.99	0.353	36.7	0.95	0.0015	59.9	0.98
	3-LDH@Mnt	1.77	3.46	0.96	0.505	28.6	0.98	0.0022	66.9	0.99
	4-LDH@Mnt	1.43	2.21	0.99	0.251	30.7	0.98	0.0031	49.3	0.97
	5-LDH@Mnt	1.62	1.13	0.99	0.242	23.1	0.99	0.0023	40.1	0.99
PQ	Mnt	0.70	1.65	0.99	0.196	12.5	0.98	0.0012	25.2	0.99
	LDH	1.04	0.01	0.99	0.260	19.6	0.98	0.0105	35.4	0.97
	1-LDH@Mnt	2.08	7.98	0.99	0.414	35.9	0.99	0.0012	65.0	0.99
	2-LDH@Mnt	2.45	6.27	0.99	0.395	44.1	0.97	0.0009	70.4	0.98
	3-LDH@Mnt	2.96	7.41	0.99	0.475	51.1	0.98	0.0009	82.0	0.99
	4-LDH@Mnt	1.84	5.71	0.99	0.351	34.1	0.96	0.0012	60.2	0.99
	5-LDH@Mnt	1.98	2.31	0.98	0.247	36.3	0.97	0.0006	54.9	0.99

(Equation 5), Freundlich (Equation 6) and Henry (Equation 7) isotherm models were employed to fit the experimental data.

$$\frac{C_e}{Q_e} = \frac{1}{K_L Q_m} + \frac{Q_e}{Q_m} \tag{5}$$

$$\log Q_e = \log K_F + \frac{1}{n}\log C_e \tag{6}$$

$$Q_e = K_d C_e \tag{7}$$

where Q_m (mg g^{-1}) is the sorption capacity or adsorption maximum of ATZ and PQ onto adsorbents, Q_e (mg g^{-1}) is the equilibrium adsorption amount, K_L (L mg^{-1}) is the Langmuir coefficient (representing the adsorption affinity), K_F ($mg^{(1-n)}/L^{-n}/g$) is the Freundlich constant, n is the coefficient related to the adsorption intensity and K_d is the Henry coefficient.

The fitted curves and related parameters are shown in Fig. 4 and Table 4, respectively. For the removal of ATZ and PQ by all adsorbents, the Langmuir isotherm model showed a much higher correlation than the Freundlich model. Thus, the fitted results suggested that the adsorption of ATZ and PQ was primarily due to monolayer adsorption, and the adsorption could take place at a finite number of localized sites. R_L is the regular parameter of Langmuir and the formula to calculate this is $R_L = 1/(1 + K_L C_0)$, which reflects the essential characteristics of the Langmuir model. The calculated R_L values are shown in Table 4. The R_L results ($0 < R_L < 1$) revealed that composite adsorbents have a favourable adsorption affinity for ATZ and PQ. Furthermore, the sorption capacities of the various adsorbent were compared, and the results are presented in Table 5. The results revealed that, in comparison with other reported adsorbents, the 3-LDH@Mnt composite exhibited a superior adsorption capacity for ATZ and PQ.

Adsorption mechanism analysis

To delve deeper into the adsorption mechanism of PQ and ATZ, we characterized the 3-LDH@Mnt samples after adsorption, as depicted in Fig. 5. In the FTIR spectra results, after adsorption of PQ the symmetric and asymmetric stretching vibration peaks of C–H appeared at 2900 and 2780 cm^{-1}, and after sorption of ATZ the stretching vibration peak of C=N at 1500 cm^{-1} was observed, indicating that PQ and ATZ were successfully adsorbed by the composite sample. The XRD traces of 3-LDH@Mnt after the adsorption of PQ and ATZ are shown in Fig. 5b. Compared with the XRD trace of 3-LDH@Mnt itself, after adsorption of PQ and ATZ no new peaks were produced, and the positions of the (003) peak did not shift, indicating that the adsorption of PQ and ATZ by LDH@Mnt was mainly *via* surface adsorption, and the contaminant did not enter the interlayers of the LDH and Mnt layers.

Although the test data regarding ATZ and PQ removal using these samples could fit the Langmuir isothermal model well, some deficiencies in understanding the sorption process remained. The Langmuir model assumes adsorption on a single-layer surface in which all adsorption sites are identical and equivalent. In other words, each adsorption site possesses equal adsorption activation energy and there is no migration between adsorbed molecules. In the composite samples, both LDH and Mnt provide adsorption sites for ATZ or PQ, but these adsorption sites are not identical. This violates the hypothesis of the Langmuir model and fails to precisely describe the sorption process. The generalized Langmuir model, which evolved from the Langmuir model, is a generalized isothermal model that considers the non-uniformity of the adsorbent. Therefore, the generalized Langmuir model was used to analyse the removal process, and three more parameters of heterogeneity (m, n) and site adsorption energy (E) were introduced. Here, the generalized Langmuir model (Equation 8) can be written as follows:

$$Q_e = Q_g^0 \left[\frac{(b_g C_e)^m}{1 + (b_g C_e)^m}\right]^{\frac{n}{m}} \tag{8}$$

where Q_g^0 is the maximum adsorption capacity, m and n are heterogeneity parameters and b is the adsorption energy-related Langmuir constant, which we defined to be <1. The fitted data and calculated correlation parameters are also shown in Fig. 4 and Table 6.

The fitted results showed that, based on the correlation coefficient (R^2) and ARE results, the generalized Langmuir model

https://doi.org/10.1180/clm.2024.4 Published online by Cambridge University Press

https://doi.org/10.1180/clm.2024.4 Published online by Cambridge University Press

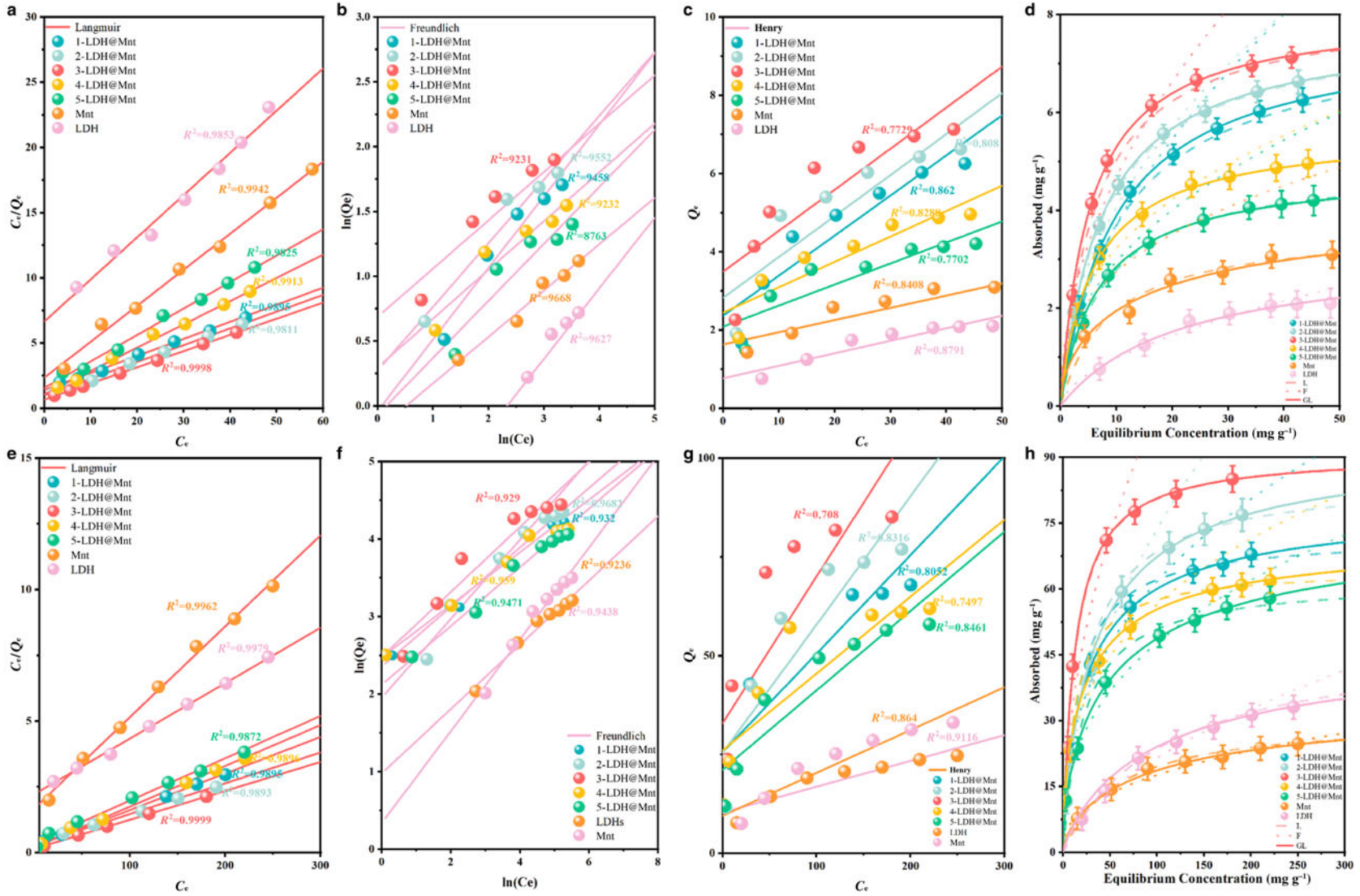

Figure 4. Isotherm study of ATZ and PQ on Mnt, LDH, 1-LDH@Mnt, 2-LDH@Mnt, 3-LDH@Mnt, 4-LDH@Mnt and 5-LDH@Mnt fitted with (a,e) Langmuir, (b,f) Freundlich, (c,g) Henry and (d,h) generalized Langmuir models.

Table 4. Fitting parameters of the Freundlich, Langmuir and Henry models of Mnt, LDH, 1-LDH@Mnt, 2-LDH@Mnt, 3-LDH@Mnt, 4-LDH@Mnt and 5-LDH@Mnt for ATZ and PQ.

Contaminant	Absorbent	Q_m (mg g-)	Langmuir				Freundlich				Henry			
			K_L (L mg^{-1})	R^2	ARE	R_L	K_F (mg$^{(1-n)}$/L^{-n}/g)	n	R^2	ARE	K_d (L mg^{-1})	R^2	ARE
ATZ	Mnt	2.05	0.11	0.98	5.2	0.15	1.20	2.79	0.97	14.9	0.0312	0.8408	12.985
	LDH	1.43	0.05	0.98	14.5	0.30	0.26	1.74	0.97	21.9	0.0320	0.8791	19.860
	1-LDH@Mnt	6.05	0.09	0.98	3.6	0.18	1.04	1.81	0.94	16.8	0.1025	0.8620	15.081
	2-LDH@Mnt	6.75	0.13	0.98	4.8	0.13	1.31	2.04	0.95	11.1	0.1047	0.8080	17.220
	3-LDH@Mnt	7.03	0.16	0.98	3.8	0.11	1.48	2.00	0.91	14.7	0.1049	0.7729	16.497
	4-LDH@Mnt	4.14	0.16	0.98	2.9	0.11	1.32	2.57	0.93	9.8	0.0649	0.8288	13.265
	5-LDH@Mnt	3.78	0.13	0.98	5.2	0.13	1.07	2.27	0.88	21.9	0.0538	0.7702	29.967
PQ	Mnt	30.7	0.02	0.98	4.1	0.13	2.86	2.54	0.97	4.8	0.0653	0.8640	17.493
	LDH	49.0	0.01	0.98	1.8	0.21	1.36	1.67	0.96	6.7	0.1085	0.9116	13.438
	1-LDH@Mnt	71.9	0.06	0.98	9.6	0.04	10.6	2.61	0.97	12.4	2.4970	0.8052	40.830
	2-LDH@Mnt	85.5	0.04	0.98	5.2	0.06	7.04	1.96	0.96	15.2	0.3249	0.8316	36.689
	3-LDH@Mnt	91.9	0.08	0.98	2.4	0.03	10.7	2.05	0.92	22.2	0.3718	0.7080	63.748
	4-LDH@Mnt	64.5	0.08	0.98	8.3	0.03	11.9	2.95	0.97	12.3	0.1948	0.7497	59.256
	5-LDH@Mnt	62.1	0.04	0.98	6.1	0.05	8.35	2.64	0.97	11.8	0.2010	0.8461	37.600

provided a better fit of the data than the Langmuir model regarding the sorption of ATZ and PQ by the compound adsorbents, revealing that the generalized Langmuir model can better describe the removal process. Therefore, adsorption of ATZ or PQ molecules proceeded *via* monolayer adsorption, but the active sites of the composite adsorbents were inhomogeneous. To further investigate the differences between the adsorption-site distributions and active-site energies, we employed site energy distribution theory.

The non-uniform energy adsorption process of the adsorbent can be studied theoretically using site energy distribution theory. This enables the calculation of the distribution function and energy of biosorption sites, indicating the binding strength of the adsorbent and the adsorption site. The integral formula can be improved to forecast the power distribution of active sites in the theory of heterogeneous surface adsorption. It is considered that the adsorption capacity $Qe(Ce)$ of the adsorbent on a non-uniform surface is equal to the integration of the adsorption isotherm $Qh(E,Ce)$ multiplied by the energy distribution function $F(E)$ of the local adsorption site with uniform energy (Equation 9).

$$Qe(Ce) = \int_0^{\infty} Qh(E, Ce)F(E)dE \tag{9}$$

In this context, the generalized Langmuir model is employed to investigate the site energy distribution during the adsorption process. The deduction process involved was presented in previous work (Xia *et al.*, 2022), and the formula yields the following results (Equations 10 & 11):

$$F(E^*) = \frac{nQ_g^0(b_gC_s)^n}{RT}\exp\left(\frac{-nE^*}{RT}\right)[1 + (b_gC_s\exp(-E^*/RT))^m]^{-\left(1+\frac{n}{m}\right)} \tag{10}$$

$$\mu(E^*) = \frac{RT}{m}\ln(1 + b_gC_s^m) \tag{11}$$

where $E^\star$ is the difference in sorption energy between the adsorbent and the adsorbent at a certain sorption site, C_s is the maximum dissolubility of the sorbent in solution and R is the gas constant.

Figure 6a,b depicts the relationship between each sample's adsorption capacity and the site energy $E^\star$ at the PQ and ATZ adsorption equilibrium point. The theory of site energy distribution explores the uneven adsorption energy process on the adsorbent from an energy perspective, revealing the power levels of the sorption sites and their distribution functions. The site energy ($E^\star$) of LDH, Mnt and LDH@Mnt composites dropped as the equilibrium adsorption capacity of ATZ and PQ increased, indicating that ATZ and PQ first selected the high-energy sites of the adsorbent in the initial stage of adsorption and preferentially occupied these high-energy sites. As the adsorption capacity increased, PQ/ATZ molecules occupied the low-energy sites on the adsorbents until all accessible locations were occupied. In the site energy distribution theory fitting results, the LDH@Mnt composite curve covered both high- and low-energy site regions, suggesting its ability to integrate the advantages of Mnt and LDH. This composite exposed additional adsorption sites through the mutual support of the LDH and Mnt layers, distinguishing it from Mnt and LDH alone. In Fig. 6a,b, the q_e–$E^\star$ curves of the

https://doi.org/10.1180/clm.2024.4 Published online by Cambridge University Press

Table 5. Comparison of the adsorption capacities for ATZ and PQ of the various adsorbents.

Contaminant	Adsorbent	Q_m (mg g^{-1})	Reference
ATZ	Biochar from corn straw	1.94	Tan *et al.* (2016)
	Biochar from *Cedrella fissilis*	5.71	Hernandes *et al.* (2022)
	Cassava waste biochar	6.12	Li *et al.* (2018)
	Alluvial soil	0.016	Yue *et al.* (2017)
	Acid-activated zeolite-rich tuffs	1.10	Salvestrini *et al.* (2010)
	Biochar from bamboo culm	2.70	Sbizzaro *et al.* (2021)
	Modified *Moringa oleifera* Lam	4.30	Cusioli *et al.* (2019)
	3-LDH@Mnt	7.03	This work
PQ	Graphene oxide with silica	29.15	Dehgani *et al.* (2020)
	Activated carbon cloth	10.28	Tongur & Ayranci (2021)
	Goethite	25.71	Iglesias *et al.* (2010)
	Mesoporous silica with titania	15.42	Brigante & Schulz (2011)
	Treated diatomaceous earth	18.00	Tsai *et al.* (2005)
	3-LDH@Mnt	91.90	This work

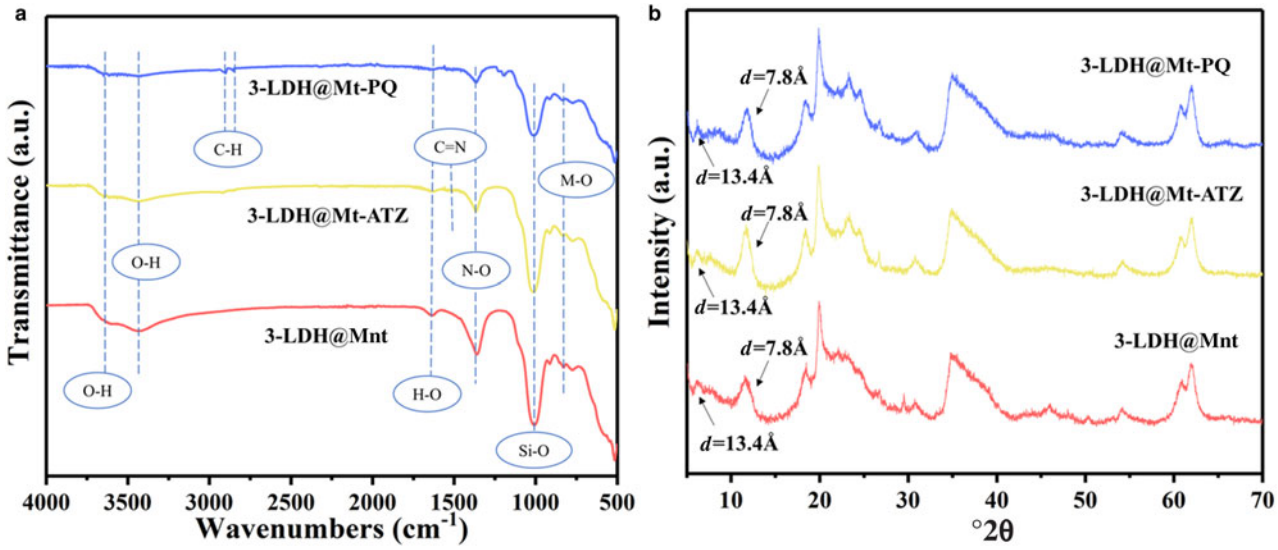

Figure 5. (a) FTIR spectra and (b) XRD traces after adsorption of ATZ and PQ on 3-LDH@Mnt.

three composite samples show similar trends, and 3-LDH@Mnt possessed more adsorption sites, in accordance with the results from the structural and shape analysis.

Table 6. Fitting parameters of the generalized Langmuir model of Mnt, LDH, 1-LDH@Mnt, 2-LDH@Mnt, 3-LDH@Mnt, 4-LDH@Mnt and 5-LDH@Mnt for ATZ and PQ.

Contaminant	Absorbent	Generalized Langmuir model					
		Q_0 (mg g^{-1})	B (L mg^{-1})	*m*	*n*	R^2	ARE
ATZ	Mnt	2.03	0.04	0.88	0.61	0.99	4.8
	LDH	1.42	0.05	1.00	1.00	0.99	12.3
	1-LDH@Mnt	6.07	0.10	1.00	1.00	0.99	2.9
	2-LDH@Mnt	6.73	0.13	1.00	0.99	0.99	4.2
	3-LDH@Mnt	7.03	0.19	0.99	1.00	0.99	3.2
	4-LDH@Mnt	4.13	0.13	0.99	0.86	0.99	2.4
	5-LDH@Mnt	3.77	0.14	0.96	1.00	0.99	4.5
PQ	Mnt	30.6	0.01	0.90	0.71	0.99	3.6
	LDH	42.6	0.01	0.87	1.00	0.99	1.2
	1-LDH@Mnt	71.9	0.02	0.90	0.65	0.99	8.2
	2-LDH@Mnt	85.4	0.02	0.92	0.81	0.99	4.5
	3-LDH@Mnt	91.9	0.07	0.99	0.91	0.99	1.8
	4-LDH@Mnt	64.5	0.02	0.90	0.54	0.99	7.6
	5-LDH@Mnt	62.2	0.01	0.81	0.69	0.99	5.5

The average site energies for the sorption of ATZ and PQ by Mnt, LDH and LDH@Mnt samples were also calculated, and the results are shown in Fig. 6c,d. LDH and Mnt have similar average site energies, which are 5.55 and 5.93 kJ mol^{-1} for ATZ and 8.63 and 8.76 kJ mol^{-1} for PQ, respectively. The calculated site energies of 1-LDH@Mnt, 3-LDH@Mnt and 5-LDH@Mnt are higher than those of LDH and Mnt, which were 7.46, 8.67 and 8.12 kJ mol^{-1} for ATZ and 11.69, 14.47 and 9.72 kJ mol^{-1} for PQ, respectively. The results demonstrate that the LDH@Mnt composite adsorbents possessed numerous adsorption sites and exhibited high adsorption energy, which are conducive to the removal of ATZ and PQ.

The effects of pH, coexistence of ions and reuse experiments

The impact of the initial pH on the adsorption effects of ATZ and PQ was investigated. The adsorption capacity of 3-LDH@Mnt for ATZ and PQ was determined at pH values ranging from 3 to 9, as shown in Fig. 7a,b. The sorption capacities for ATZ and PQ at pH 3 and 5 were much greater than those at pH 7 and 9, revealing that the adsorption effect under acidic conditions was better than that under neutral or basic conditions. Under acidic conditions, on account of the protonation reaction with ATZ/PQ

https://doi.org/10.1180/clm.2024.4 Published online by Cambridge University Press

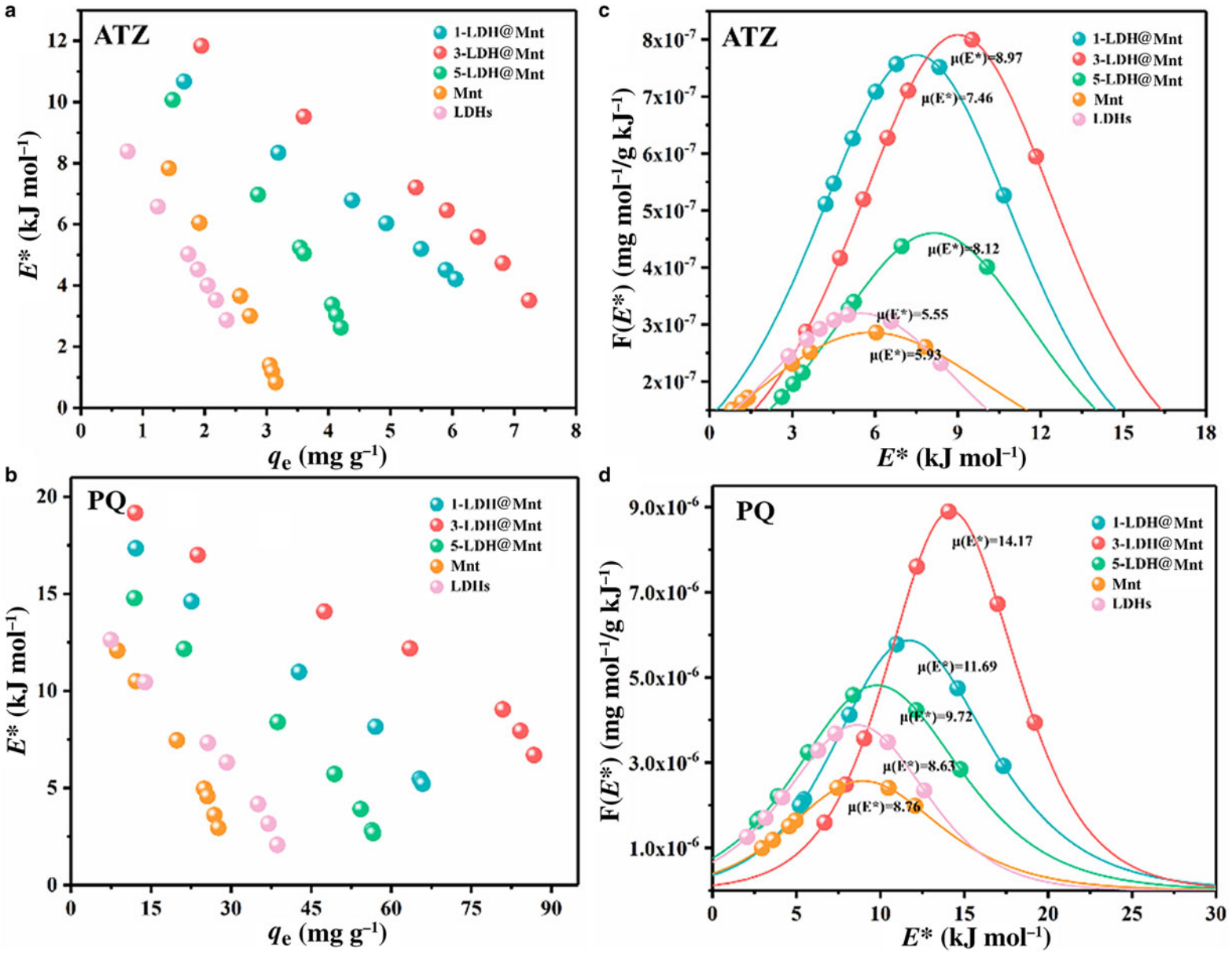

Figure 6. The distributions and site energies for (a,c) ATZ and (b,d) PQ adsorption on Mnt, LDH, 1-LDH@Mnt, 3-LDH@Mnt and 5-LDH@Mnt.

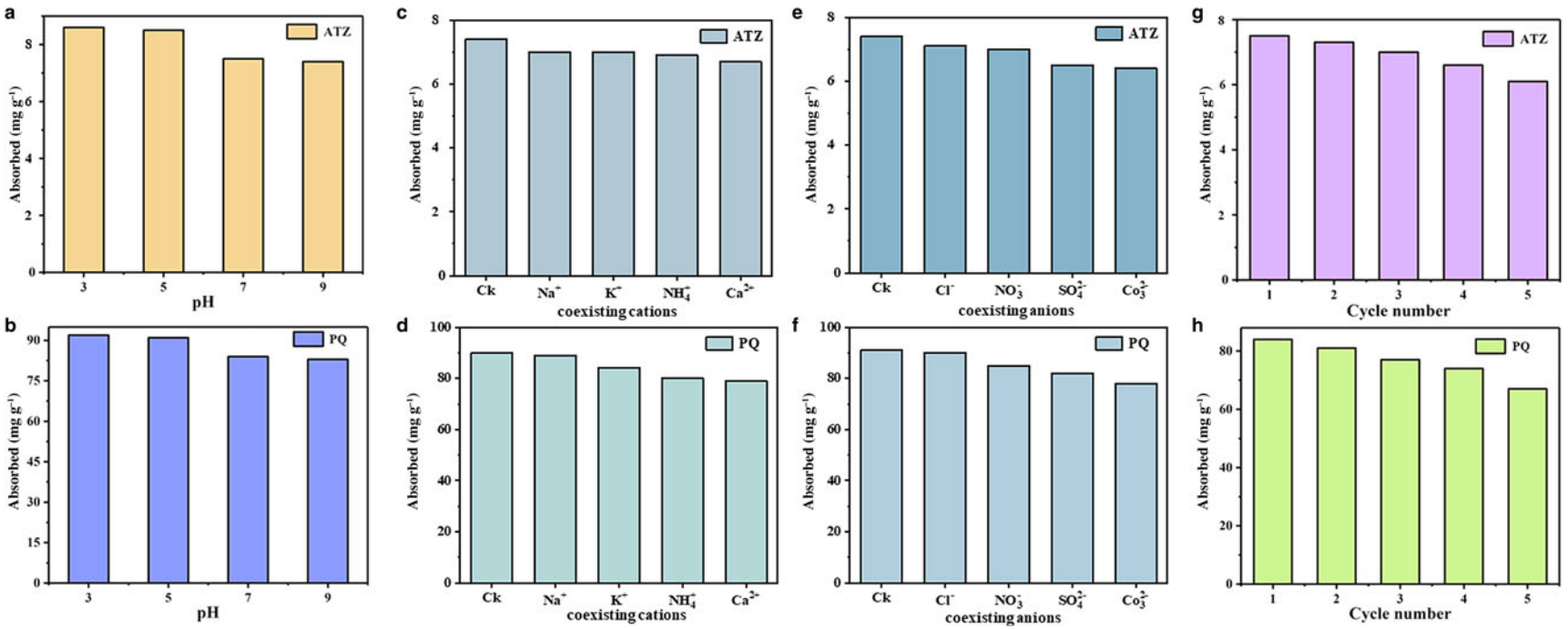

Figure 7. Effect of (a,b) initial pH, (c–f) coexisting cations and anions and (g,h) reuse experiments on ATZ and PQ adsorption on 3-LDH@Mnt.

molecules, ATZ/PQ in the form of cations was attracted to the negatively charged layers of Mnt and reduced the electrostatic repulsion with the LDH@Mnt composite, which was conducive to the removal of ATZ and PQ. However, under alkaline conditions, the concentration of H^+ was decreased, and the protonation reaction of ATZ/PQ molecules was weakened, resulting in the adsorption amount for ATZ and PQ being decreased slightly.

The effect of coexisting anions on the sorption of ATZ and PQ by 3-LDH@Mnt was also assessed, and the results are shown in Fig. 7c–f. The presence of Na^+, K^+, Mg^{2+} and Ca^{2+} cations and Cl^-, NO^{3-}, SO_4^{2-} and CO_3^{2-} anions did not exert much influence on the removal of ATZ and PQ, revealing that the LDH@Mnt composite possessed high adsorption stability and was reliable for the adsorption ATZ and PQ in various environmental systems. The reuse capability of 3-LDH@Mnt was also experimentally explored, and the results are shown in Fig. 7g,h. After five cycles, the adsorption amount was reduced to 6.32 mg g^{-1} for ATZ and 70.8 mg g^{-1} for PQ; however, the removal rates of ATZ and PQ still exceeded 70%, demonstrating the good reusability and continuous effective adsorption performance of the composite.

Conclusion

In this study, Mnt modified with varying amounts of LDH was successfully synthesized using the *in situ* method. The XRD and FTIR spectroscopy results revealed that the LDH structure was successfully combined with Mnt. From the BET and SEM results, LDH loaded on the surface of Mnt layers could form porous structures and increase the specific surface area; however, excess LDH caused the aggregation and accumulation on the layers. The adsorption kinetic data revealed that the biosorption process well fitted the quasi-second-order model and internal diffusion model. The composite sample 3-LDH@Mnt possessed the best adsorption efficiency for both ATZ and PQ, and the adsorption capacities were 7.03 and 91.9 mg g^{-1}, respectively. These adsorption amounts indicate that the biosorption process was influenced by the number of active sites of the adsorbent. The XRD and FTIR spectroscopy results after adsorption indicated that the removal of PQ and ATZ by LDH@Mnt was mainly *via* surface adsorption. In the study of the adsorption isotherm, the generalized Langmuir model accurately characterized the adsorption of ATZ and PQ, revealing that the adsorbents had a certain number of active sites but their energy levels differed. According to the assumption of site energy distribution, the composite adsorbent had a significant number of biosorption sites and the sorption energy was high, both of which being beneficial for the removal of ATZ and PQ. The influence of pH, coexisting ions and reuse experiments demonstrated the high adsorption stability of the LDH@Mnt composite, indicating that it represents a reliable choice for ATZ and PQ adsorption in various environmental systems. The results also show that the adsorption effect of the composite of Mnt and LDH is better than that of the two materials alone. The composite adsorbent points the way towards the development of a series of efficient adsorption materials and will help future studies to improve the adsorption effects of clay minerals. It also has crucial practical implications for environmental protection.

Supplementary material. The supplementary material for this article can be found at https://doi.org/10.1180/clm.2024.4.

Data availability. All data used in this study, including the training datasets, can be found in the Supplementary Materials.

Acknowledgements. The authors thank the anonymous reviewers and the editor, Professor Chun-Hui Zhou, for constructive suggestions and comments on this work.

Financial support. This research was supported by the National Natural Science Foundation of China (Grant Nos. 42102076) and project ZR2021QD037 supported by Shandong Provincial Natural Science Foundation.

Conflicts of interest. The authors declare none.

References

Ajala O.J., Nwosu F.O. & Ahmed R.K. (2018) Adsorption of atrazine from aqueous solution using unmodified and modified bentonite clays. *Applied Water Science*, **8**, 214.

Al Kausor M., Sen Gupta S., Bhattacharyya K.G. & Chakrabortty D. (2022) Montmorillonite and modified montmorillonite as adsorbents for removal of water soluble organic dyes: a review on current status of the art. *Inorganic Chemistry Communications*, **143**, 109686.

Alexe-Ionescu A.L., Zaccagnini P., Lamberti A., Pirri C.F. & Barbero G. (2019) Generalized langmuir kinetic equation for ions adsorption model applied to electrical double layer capacitor. *Electrochimica Acta*, **323**, 134700.

Boutaleb N., Chouli F., Benyoucef A., Zeggai F.Z. & Bachari K. (2021) A comparative study on surfactant cetyltrimethylammoniumbromide modified clay-based poly(p-anisidine) nanocomposites: synthesis, characterization, optical and electrochemical properties. *Polymer Composites*, **42**, 1648–1658.

Brigante M. & Schulz P.C. (2011) Adsorption of paraquat on mesoporous silica modified with titania: effects of pH, ionic strength and temperature. *Journal of Colloid and Interface Science*, **363**, 355–361.

Buchanan G.A. & Hiltbold A.E. (2017) Performance and persistence of atrazine. *Weed Science*, **21**, 413–416.

Centner T.J. (2021) Pesticide usage is compromising people's health in the United States: ideas for reducing damages. *Agriculture*, **11**, 486.

Chen L., Li C., Wei Y., Zhou G., Pan A., Wei W. & Huang B. (2016) Hollow LDH nanowires as excellent adsorbents for organic dye. *Journal of Alloys and Compounds*, **687**, 499–505.

Chen X., Zhou Q., Liu F., Peng Q. & Teng P. (2019) Removal of nine pesticide residues from water and soil by biosorption coupled with degradation on biosorbent immobilized laccase. *Chemosphere*, **233**, 49–56.

Dabizha A. & Kersten M. (2022) Aqueous solubility of Zn incorporated into Mg–Al-layered double hydroxides. *Clays and Clay Minerals*, **70**, 34–47.

Dehgani Z., Sedghi asl M., Ghaedi M., Sabzehmeidani M.M. & Adhami E. (2020) Removal of paraquat from aqueous solutions by a bentonite modified zero-valent iron adsorbent. *New Journal of Chemistry*, **44**, 13368–13376.

Durán E., Bueno S., Hermosín M.C., Cox L. & Gámiz B. (2019) Optimizing a low added value bentonite as adsorbent material to remove pesticides from water. *Science of the Total Environment*, **672**, 743–751.

Glaberman S., Padilla S. & Barron M.G. (2017) Evaluating the zebrafish embryo toxicity test for pesticide hazard screening. *Environmental Toxicology and Chemistry*, **36**, 1221–1226.

Hernandes P.T., Franco D.S.P., Georgin J., Salau N.P.G. & Dotto G.L. (2022) Investigation of biochar from *Cedrella fissilis* applied to the adsorption of atrazine herbicide from an aqueous medium. Journal of Environmental *Chemical Engineering*, **10**, 107498.

Huang L., Wang L., Wang C. & Tao X. (2022) Effect of intercalation of flocculant on adsorption properties of ZnMgAl-LDHs. *Inorganic Chemistry Communications*, **135**, 109127.

Iglesias A., Lopez R., Gondar D., Antelo J., Fiol S. & Arce F. (2010) Adsorption of paraquat on goethite and humic acid-coated goethite. *Journal of Hazardous Materials*, **183**, 664–668.

Ionel I.L., Mara G., Stefania R., Margarita G.O. & Corina P. (2019) A hazard to human health – pesticide residues in some vegetal and animal foodstuff. *Journal of Biotechnology*, **305**, S22–S23.

la Cecilia D. & Maggi F. (2016) Kinetics of atrazine, deisopropylatrazine, and deethylatrazine soil biodecomposers. *Journal of Environmental Management*, **183**, 673–686.

Li X., Luo J., Deng H., Huang P., Ge C., Yu H. & Xu W. (2018) Effect of cassava waste biochar on sorption and release behavior of atrazine in soil. *Science of the Total Environment*, **644**, 1617–1624.

Liao K., An J., Fu L., Zhang H., Wei M., Bai J. & He Y. (2022) Adsorption of welan gum on montmorillonite and its influencing factors. *Polymers*, **14**, 2599.

Liu L., Zhang Y.-J., Xia Z.-Q., Li S.-B. & Wang N. (2022) Triple-shelled nico-LDH@CoFe-PBA@NiCo-LDH hollow cubes for efficient adsorption property toward anionic organic pollutant. *Materials Letters*, **312**, 131647.

Mandal A., Singh N. & Purakayastha T.J. (2017) Characterization of pesticide sorption behaviour of slow pyrolysis biochars as low cost adsorbent for atrazine and imidacloprid removal. *Science of the Total Environment*, **577**, 376–385.

Mennas N., Lahreche S., Chouli F., Sabantina L. & Benyoucef A. (2023) Adsorption of Methylene Blue dye by cetyltrimethylammonium bromide intercalated polyaniline-functionalized montmorillonite clay nanocomposite: kinetics, isotherms, and mechanism study. *Polymers*, **15**, 3518.

Salvestrini S., Sagliano P., Iovino P., Capasso S. & Colella C. (2010) Atrazine adsorption by acid-activated zeolite-rich tuffs. *Applied Clay Science*, **49**, 330–335.

Semenkova A.S., Evsiunina M.V., Verma P.K., Mohapatra P.K., Petrov V.G., Seregina I.F. *et al.* (2018) Cs^+ sorption onto kutch clays: influence of competing ions. *Applied Clay Science*, **166**, 88–93.

Siddique S., Chaudhry M.N., Ahmad S.R., Nazir R., Zhao Z., Javed R. *et al.* (2023) Ecological and human health hazards; integrated risk assessment of organochlorine pesticides (OCPS) from the Chenab River, Pakistan. *Science of the Total Environment*, **882**, 163504.

Silva D.T.C., Fonseca M.G., Borrego-Sánchez A., Soares M.F.R., Viseras C., Sainz-Díaz C.I. & Soares-Sobrinho J.L. (2020) Adsorption of tamoxifen on montmorillonite surface. *Microporous and Mesoporous Materials*, **297**, 110012.

Tao X., Liu D., Cong W. & Huang L. (2018) Controllable synthesis of starch-modified ZnMgAl-LDHs for adsorption property improvement. *Applied Surface Science*, **457**, 572–579.

Tao X., Liu D., Song J., Ye Q. & Xu D. (2017) Plasma modification of ZnMgAl-LDHs for adsorption property improvement. *Journal of the Taiwan Institute of Chemical Engineers*, **74**, 281–288.

Tian Y., Xie J., Zhang F., Xu L. & Zhao Z. (2023) Synthesis and lithium adsorption performance of $NiFe_2O_4$@AlLi-LDH. *Journal of Sustainable Metallurgy*, **9**, 1075–1083.

Tongur T. & Ayranci E. (2021) Adsorption and electrosorption of paraquat, diquat and difenzoquat from aqueous solutions onto activated carbon cloth as monitored by *in-situ* UV–visible spectroscopy. *Journal of Environmental Chemical Engineering*, **9**, 105566.

Tsai W.T., Hsien K.J., Chang Y.M. & Lo C.C. (2005) Removal of herbicide paraquat from an aqueous solution by adsorption onto spent and treated diatomaceous earth. *Bioresource Technology*, **96**, 657–663.

Uygun O., Murat A. & Çakal G.Ö. (2023) Magnetic sepiolite/iron(III) oxide composite for the adsorption of lead(II) ions from aqueous solutions. *Clay Minerals*, **58**, 267–279.

Valbuena D., Cely-Santos M. & Obregon D. (2021) Agrochemical pesticide production, trade, and hazard: narrowing the information gap in Colombia. *Journal of Environmental Management*, **286**, 112141.

Vasseghian Y., Arunkumar P., Joo S.-W., Gnanasekaran L., Kamyab H., Rajendran S. *et al.* (2022) Metal–organic framework-enabled pesticides are an emerging tool for sustainable cleaner production and environmental hazard reduction. *Journal of Cleaner Production*, **373**, 133966

Wu L., Sun M., Wang X., Lu Y., Tang N., Gao L. *et al.* (2023) Preparation and corrosive anion-curing capability of layered double hydroxide (LDH)/montmorillonite composites. *Clays and Clay Minerals*, **71**, 461–477.

Xia C., Huang H., Liang D., Xie Y., Kong F., Yang Q. *et al.* (2022) Adsorption of tetracycline hydrochloride on layered double hydroxide loaded carbon nanotubes and site energy distribution analysis. *Chemical Engineering Journal*, **443**, 136398.

Yue L., Ge C., Feng D., Yu H., Deng H. & Fu B. (2017) Adsorption–desorption behavior of atrazine on agricultural soils in China. *Journal of Environmental Sciences*, **57**, 180–189.

Zheng D., Wu M., Zheng E., Wang Y., Feng C., Zou J. *et al.* (2022) Parallel adsorption of low concentrated ciprofloxacin by a CoFe-LDH modified sludge biochar. *Journal of Environmental Chemical Engineering*, **10**, 108381.

https://doi.org/10.1180/clm.2024.4 Published online by Cambridge University Press